

Article

Pinning Effect of Cerium Inclusions during Austenite Grains Growth in SS400 Steel at 1300 °C: A Combined Phase Field and Experimental Study

Zary Adabavazeh, Weng-Sing Hwang * and Amir R. A. Dezfoli

Department of Materials Science and Engineering, National Cheng Kung University, Tainan 701, Taiwan; zary.adabavazeh@yahoo.com (Z.A.); Ansari_amirreza@yahoo.com (A.R.A.D.)

* Correspondence: wshwang@mail.ncku.edu.tw; Tel.: +886-062344393

Academic Editor: Helmut Cölfen

Received: 12 September 2017; Accepted: 11 October 2017; Published: 15 October 2017

Abstract: The pinning effect of cerium inclusions in the austenite grain growth of SS400 steel at 1300 °C is investigated by using a semi-empirical-simulation. Firstly, steel samples containing cerium inclusions are prepared; then the properties of inclusions are determined using SEM. In situ observation of austenite grain growth is performed by LSCM, to determine the fitting parameters of the model such as the grain mobility and the pinning parameter. These parameters are directly inserted into our phase field simulation. The time-dependent Ginzburg-Landau (TDGL) equation is implemented in our phase field model, where the effects of inclusion and grain boundary interaction are inserted as a potential term in the local free energy. The results proved that the optimal size of austenite grains can be achieved by changing the volume fraction of inclusions. In fact, by increasing the volume fraction of inclusions from 0 to 0.1, the austenite grain growth can be decreased where the boundary mobility reduces from $2.3 \times 10^{-12} \text{ m}^4/\text{Js}$ to $1.0 \times 10^{-12} \text{ m}^4/\text{Js}$. The results also demonstrated that increasing the temperature can provide more energy for grain to overcome the inclusions' pinning force. Moreover, it was shown that the classical Zener model, $R_c = 0.45r_p f_i^{-1}$, describes the pinning effect of cerium inclusions.

Keywords: SS400 steel; semi-empirical-simulation; austenite grain growth; pinning effect; cerium inclusions

1. Introduction

SS400 steel is a constructional grade ferritic-pearlitic steel [1]. This kind of steel has wide applications in land vehicles and structures. One of the heat treatment processes of steel and other ferrous alloys is the austenitization process, where these materials are heated above their critical temperatures long enough for a ferrite to austenite transformation to take place [2,3]. The purpose of austenitizing steel and other ferrous alloys is to transform them into the required shape and provide proper strength and resistance to the material [2]. In fact, changing the phase from ferrite to austenite can happen from 912 °C to ~1400 °C, when the Body Centered Cubic (BCC) phase changes to the Face-Centered Cubic (FCC) austenite steel (gamma steel) [4].

To date, different studies have been performed to investigate the controlling of the austenite grain size during the austenitizing process of the steels [5–8]. The reason of these numerous interests is the important impact of grain size on diffusive and diffusionless phase transformations, precipitation, and mechanical properties such as toughness, ductility, strength, and hardness [7]. Increasing the grain size will result in the reduction of these mechanical properties. Moreover, very small grains decrease the hardenability of the steel. As a result, the proper size of grains is desired to reach to proper mechanical properties [7,9]. The problem is that grain growth can easily occur after the reverse transformation

during the austenitization process, even for fine austenite grain sizes, which in turn decreases the grain boundary free energy by thermally activated atomic processes. As a result, controlling the grain growth rate presents an important issue for many researchers. Adding alloying elements in carbon steel to reduce the grain growth rate due to the pinning of grain boundaries by means of inclusions can be one of the promising methods in this regard [7,9–11].

In order to determine or modify the final properties of steel, austenite grain morphology and austenite average grain size are important parameters that need to be taken into consideration. In fact, during the cooling process from the austenitization temperature to the room temperature, the ferrite phase is homogeneously nucleated on the grain boundaries, edges, and corners [5,11]. Therefore, fewer grain boundaries, corners, and edges lead to a lower ferrite nucleation rate. During austenitization, the normal grain growth behavior is governed in the steel [5]. The normal grain growth means there are different grains with different crystallographic orientations. At high temperatures, small grains shrink and large grains grow larger [12].

Recently, much attention has been drawn to using different simulation techniques such as phase-field modeling in order to predict the microstructure and estimate the grain size in grain growth, for instance [6,12–14]. Investigating the growth laws of austenite and establishing the mathematical model to predict grain growth behavior under different temperatures and holding times are thus necessary [15]. More investigations on the kinetic metallurgical transformation is needed to gain a well-microstructured product. The effect of adding cerium on the microstructure and morphology of Ce-based inclusions formed in low-carbon steel was discussed in our previous paper [16]. In this study, the 2D kinetics of grain growth is studied using many orientation field variables obtained by solving the time-dependent Ginzburg-Landau (TDGL) equations [13]. The grain boundary mobility, M , is obtained using the fitting parameter for experimental values of interface motion extracted from the in situ observation of austenite grain growth under confocal microscopy.

2. Procedure

2.1. Phase Field Model

In this study, phase field modeling is used to simulate the grain growth. The phase of steel during the austenite grain growth is considered as a single phase. In this condition, the microstructure can be reproduced by a set of p phase-field variables:

$$\eta_1(x, t), \eta_2(x, t), \dots, \eta_p(x, t) \quad (1)$$

where x indicates space and t denotes time. The phase-field variables, η , are continuous in space and time. The time-dependent Ginzburg-Landau equation is used to calculate the evolution of the phase field variables [12,17]:

$$\frac{\partial \eta_i(x, t)}{\partial t} = -M \frac{\delta F}{\delta \eta_i(x, t)}, \quad i = 1, 2, \dots, p \quad (2)$$

where F is the free energy and M is the grain mobility. Inside the grain i labelled by η_i , the value for η_i is considered 1, and through the boundary the value of η_i changes from 1 to 0. Furthermore, inside the grain i , the value of all other phase field variables $\eta_j (j \neq i)$ is zero. The free energy, F , is a function of the phase-field variables and their gradients, which are defined as below [12]:

$$\frac{\partial \eta_i(x, t)}{\partial t} = -M \frac{\delta F}{\delta \eta_i(x, t)}, \quad i = 1, 2, \dots, p \quad (3)$$

where k_i is the gradient energy coefficient and f_0 is the local free energy density. f_0 should be defined in such a way that p minima with equal depth, f_{min} , is located at $(\eta_1, \eta_2, \dots, \eta_p) = (1, 0, \dots, 0)$,

$(0, 1, \dots, 1), \dots, (0, 0, \dots, 1)$, and takes into account the grain boundary and inclusion interactions. Here, the local free energy is defined as below [14]:

$$f_0 = \sum_{i=1}^p \left(\frac{\eta_i^4}{4} - \frac{\eta_i^2}{2} \right) + \sum_{i=1}^p \sum_{j \neq i}^p \eta_i^2 \eta_j^2 + \varphi(x)^2 \sum_{j \neq i}^p \eta_i^2, \quad (4)$$

In this definition, $\varphi(x)$ is greater than zero inside the inclusions and zero outside them. For $\varphi(x) > 0$, f_0 has a minimum at $(\eta_1, \eta_2, \dots, \eta_p) = (0, 0, \dots, 0)$. Finally, using Equations (1)–(4), the reaction–diffusion partial differential equations can be rewritten as below:

$$\frac{\partial \eta_i(x,t)}{\partial t} = -M \left(k \nabla^2 \eta_i(x,t) - \eta_i^3(x,t) + \eta_i(x,t) - 2\eta_i(x,t) \left(\sum_{j \neq i}^p \eta_j^2(x,t) + \varphi(x)^2 \right) \right), \quad i = 1, 2, \dots, p \quad (5)$$

For all the simulations, a 200×200 grid is made where p , Δt , and Δx are considered as 20,000, 0.1 s, and $5 \mu\text{m}$, respectively. In fact, Δx is considered as the average inclusion size. The gradient energy coefficient, k_i , and the pinning parameter, $\varphi(x)$, are treated as the fitting parameters, which are adjusted so that the average γ grain size coincides with the experimental value. In addition, the initial grain size is also selected based on experimental observations. As shown in Figure 1, the pinning effect only applies to the grain boundaries if the grain boundaries meet the grid including the inclusion.

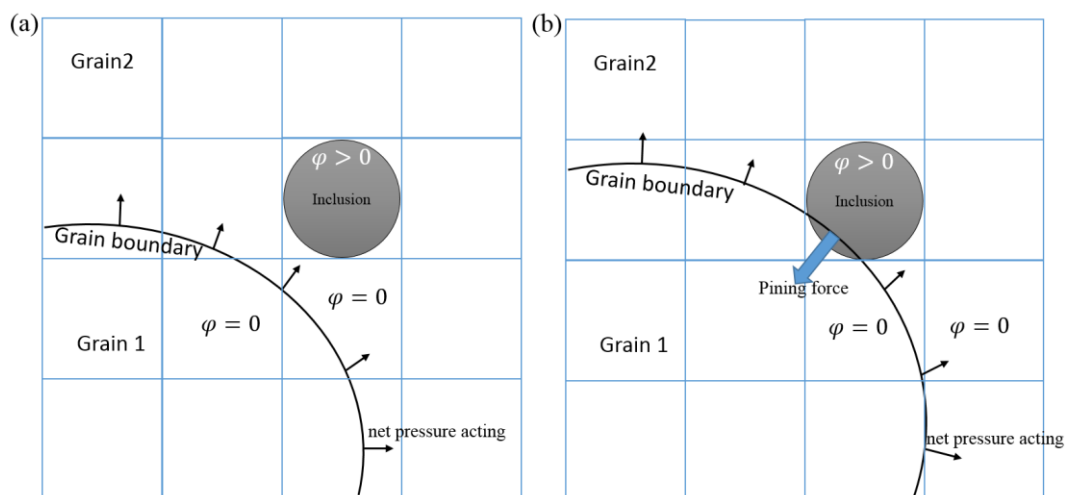


Figure 1. The pinning effect act on the grain boundaries (a) before the grain boundaries reach the inclusion, (b) after the grain boundaries meet the inclusion.

2.2. Experimental Procedure

A wide range of samples with different amount of cerium are prepared. To prepare the samples, a vacuum induction furnace (100 kHz) is used to melt commercial SS400 steel at 1873 K. Then, the melt was deoxidized by adding different amount of cerium powder wrapped in pure aluminum foil (99.99%). The whole process is conducted under an argon gas atmosphere. Changing the S/O ratio results in controlling the type of inclusions. Finally, the furnace power is turned off and the crucible with the melt is slowly cooled down in the furnace, and then quenched with water. More details about the composition of all samples can be found on our previous work [16]. In this paper, we used the sample with 235 ppm cerium, with the composition of 0.201 C, 1.300 Mn, 0.400 Si, 0.200 Al, 0.0060 P, 0.0049 S, and 0.0007 O.

In order to determine the inclusion properties, samples are ground and polished using a diamond compound to be prepared for performing SEM-EDS. Then, inclusions properties are determined by means of SEM (JSM-6301F, Japan Electronics Corporation, Tokyo, Japan) equipped with energy

dispersive X-ray spectroscopy (EDX). Cubic samples with a size of $1 \times 1 \times 1 \text{ cm}^3$ are cut from steel samples. Then, the samples are ground and polished carefully using 3 and 1 μm diamond compounds. Laser Scanning Confocal Microscopy (LSCM) is used to carry out the in situ observation of microstructure transformation on cylindrical specimens, 7 mm in diameter and 5 mm in length. Then, the surface of samples is ground and polished to minimize the surface roughness. The samples are heated in LSCM under the argon atmosphere to avoid oxidation. The heating rate is considered to be $5 \text{ }^\circ\text{C/s}$ while samples are kept at $1300 \text{ }^\circ\text{C}$ for 20 min. After in situ observation, the samples are cooled to room temperature. Metallographic observations are carried out on the specimens subjected to the casted state. The statistics of grain size and inclusions are examined by using image statistical analysis.

Figure 2 shows the flow chart to summarize the approach used in this study for the simulation of the pinning effect of cerium inclusions on austenite grain growth. Some assumptions for coupling experiments and the phase field model are considered as below:

- Inclusions have a spherical shape.
- The pinning effect only acts on boundaries when grain boundaries meet the inclusion, otherwise the pinning force is zero.
- The size of the inclusion is similar or equal to the average size of the inclusion detected by the experiments.
- Inclusions are randomly distributed.

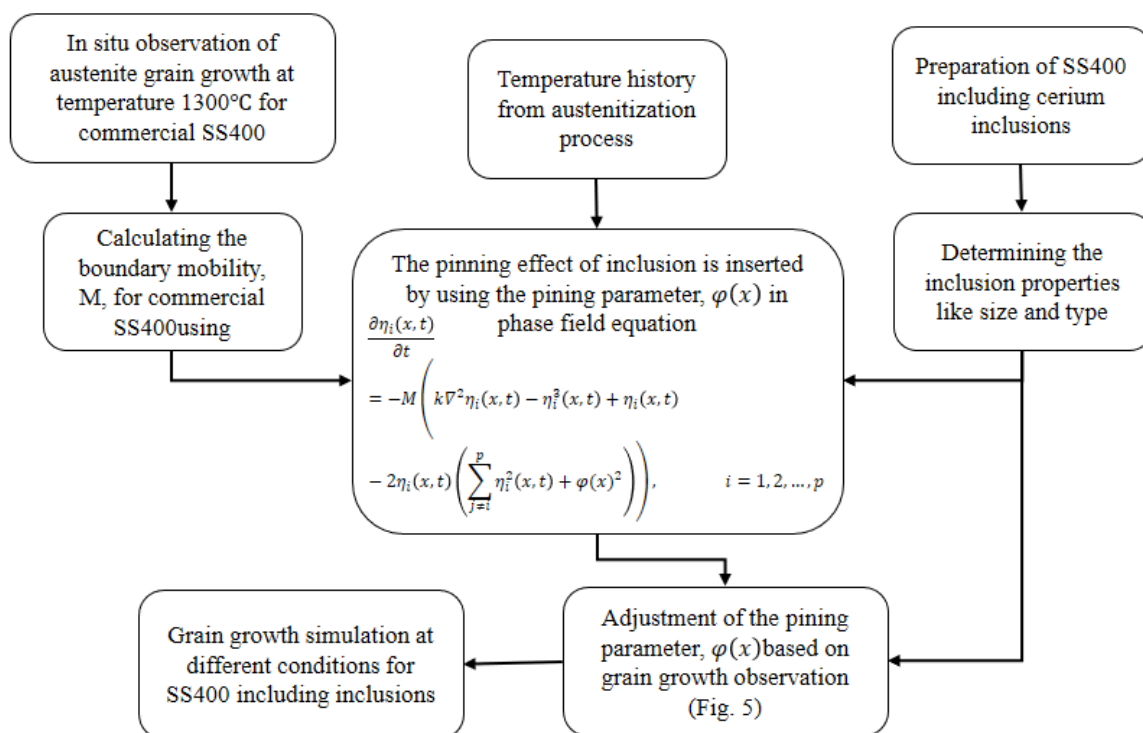


Figure 2. Schematic diagram of the pinning effect of inclusions in austenite grain growth in SS400 steel.

3. Discussion

3.1. Inclusion Properties

The SEM results proved that the inclusions were mainly $\text{Ce}_2\text{O}_2\text{S}$, CeO_2 , and Ce_2O_3 , with an average diameter of $5 \mu\text{m}$. Figure 3 shows the morphology of inclusions inside the SS400. Moreover, samples with different inclusion volume fractions were obtained by adding different amounts of

cerium, where the inclusion volume fraction can be changed from 0 (commercial SS400) to 0.1 (with a high amount of cerium added).

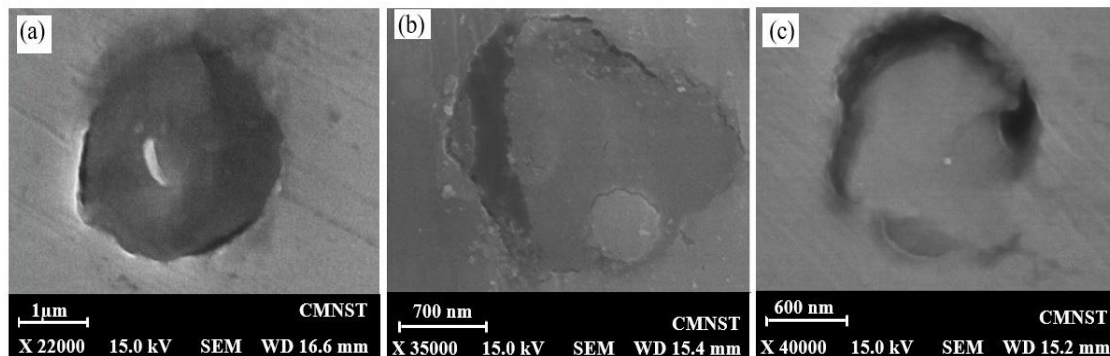


Figure 3. Inclusions morphology: (a) CeO₂ inclusion, (b) Ce₂O₃ inclusion, (c) Ce₂O₂S inclusion.

3.2. The Boundary Mobility

At austenite temperature, the boundary moves as a result of acting driving pressure, P . The velocity of boundary is given as [18]:

$$v = MP \quad (6)$$

where M is the boundary mobility. The boundary mobility is a function of temperature and can be expressed by Equation (7) [18]:

$$M = M_0 \exp\left(\frac{-Q}{RT}\right) \quad (7)$$

where T is temperature, M_0 is a constant, Q is the activation energy for boundary migration, and R is the gas constant. The velocity of the grain boundary depends on the net pressure acting on the grain boundary, given by [19]:

$$P = \alpha \frac{\gamma}{D} \quad (8)$$

D is the mean volumetric grain diameter, α is the dimensionless geometric constant, and γ is the grain boundary energy. The boundary mobility can be determined by the in situ observation of grain growth using LSCM. In this study, the changing of austenite grain size for samples is calculated for the samples held at 1300 °C for 20 min. Then, using the following equation, the velocity of the grain boundary is calculated:

$$v = \frac{1}{2} \frac{dD}{dt} \quad (9)$$

The corresponding driving pressure for boundary migration is also calculated by Equation (8). The boundary velocity is linearly proportional to the driving force and the slop of this line is the boundary mobility. In this condition, the boundary mobility at austenite temperature 1300 °C is found to be $2.3 (\times 10^{-12}) \text{ m}^4/\text{Js}$. More details on the procedure of the boundary mobility calculations can be found in Figure 2. The initial commercial SS400 grain size and the grain size after 20 min heating at 1300 °C are shown in Figure 4. The initial grain size and grain size at the end of austenitization are found ~ 85 and $\sim 97 \mu\text{m}$, respectively. The results show that large grains start to grow while small grains will shrink.

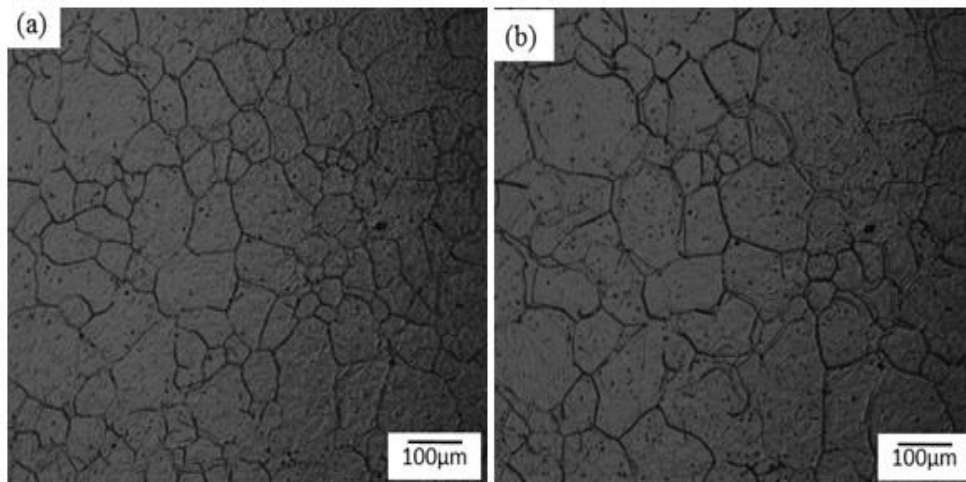


Figure 4. Grain size of commercial SS400 (a) at the beginning of austenitization and (b) after 20 min.

3.3. Adjusting the Simulation

The size of inclusions is obtained from SEM, while the inclusion location and initial austenite grain size is obtained by LSCM. Grain mobility obtained from in situ observation and temperature history for austenitization are inserted into our simulation. Then, the grain size and inclusion position related to grain boundaries are compared between the simulation and in situ observations. For $\varphi = 2$, the experimental results and simulation show the same behavior. One of the corresponding results of this linking is demonstrated in Figure 5.

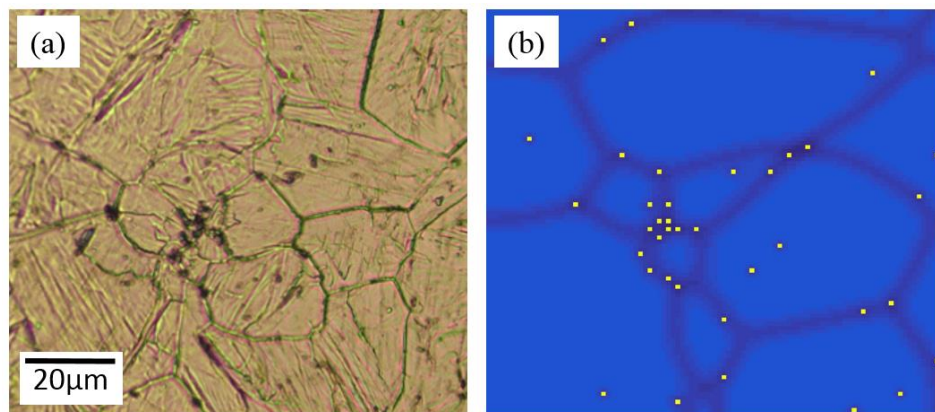


Figure 5. Comparison between experimental and simulation results for $\varphi = 2$: (a) in-situ observation, and (b) simulation results.

For both the simulation and experiment, the inclusions are located on the grain boundary more than inside the grains. This proves that inclusions interact with the grain boundary. In fact, during grain growth, the inclusions have a strong pinning effect on the grain boundaries. If the grain boundaries do not have enough driving energy, grain growth will stop. Figure 6 shows two real inclusions located on the grain boundaries observed by SEM.

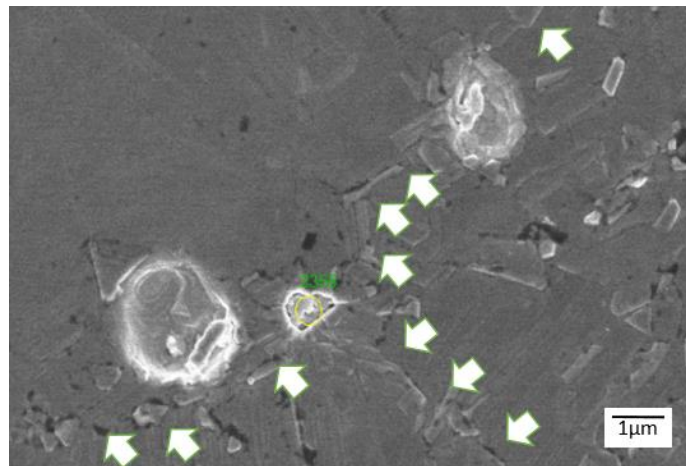


Figure 6. Interaction between grain boundaries and inclusions obtained by SEM.

3.4. The Effect of Inclusion Volume Fraction

In order to investigate the inclusion volume fraction, three different simulations were performed for f_i equal to 1, 0.05, 0.03. The grain morphology was simulated at 1300 °C and held for 1200 s. All other parameters were set as described before. Figure 7 shows the grain structure for different volume fractions of inclusions. The results show that as the volume fraction of inclusions increases, the final grain size decreases. In fact, due to the presence of inclusions, the grain boundary movements face barriers. When the grain boundary reaches the inclusion, the inclusion applies force on it. Then, the grain boundary needs more driving force to overcome the effect of inclusion. More inclusions result in the application of a greater pinning effect on the grain boundaries and consequently a decrease in grain growth. The results shown in Figure 7f reveal an interesting issue. By increasing the volume fraction of inclusions, the variation in the grain size distribution decreases. This means that, although the presence of inclusions leads to a reduction in grain size, at the same time the grain size is more homogenous. The boundary mobility is also shown in Figure 7f. Obviously, the inclusion decreases the grain boundary mobility as expected.

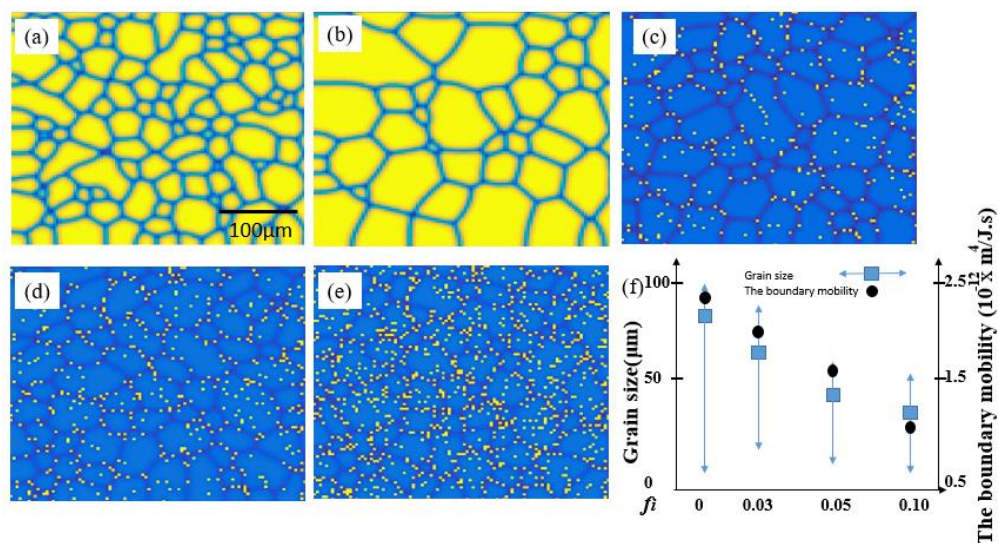


Figure 7. (a) Initial simulated grain structure, and simulated grain structure after holding for 1200 s at 1300 °C (b) for $f_i = 0$, (c) $f_i = 0.03$, (d) $f_i = 0.05$, and (e) $f_i = 1$. (f) The relationship between grain size and grain size variation with inclusion volume fraction.

3.5. The Effect of Temperature on Grain Growth

Figure 8 shows the grain morphology of SS400 held for 600 s at temperatures of 1300, 1250, and 1100 °C. For all cases, the volume fraction of inclusions is 3. Moreover, the location of the inclusions is random and the same for all three temperatures. The points indicated by the white arrows show clear differences between the grain evolutions at different temperatures. It seems that at higher temperatures, grains have more driving force to overcome the inclusion drag force. At lower temperatures, grains do not have enough driving energy to pass the inclusions. Another interesting issue is the location of inclusions is related to the grains. The inclusions are located not only at the meeting points of two grains, but also at those of three or four grains.

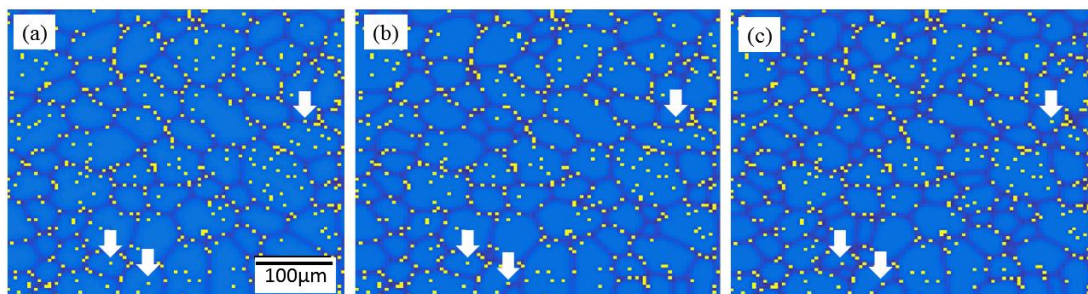


Figure 8. Grain morphology for 600 s austenitization at temperatures of (a) 1300 °C, (b) 1250 °C, and (c) 1100 °C.

3.6. Zener Pinning Model

According to the Zener pinning prediction [20,21], normal grain growth is inhibited when the grain radius reaches a critical value of R_c [22]:

$$R_c = \frac{r_p K}{f_i} \quad (10)$$

where r_p is the inclusions radius (here 2.5 μm), f_i is the volume fraction of inclusions, and K is a constant value. According to our simulation K is approximately 0.45. Then the critical value for modified SS400 with a 5-μm cerium inclusion at 1300 °C is $0.45 \frac{r_p}{f_i}$.

4. Conclusions

A combined phase field and experimental study is presented in this work. SS400 commercial steel is modified by adding cerium in order to produce different types of inclusions inside it. To determine the properties of the inclusions and austenite grains, different characterization methods are applied, including LSCM for in situ observation and SEM analysis for the determination of the size and type of inclusions. A semi-empirical-simulation is performed to investigate the pinning effect of inclusions on austenite grain growth. This pinning effect is found to be strong enough to decrease grain growth at 1300 °C. In addition, the results showed that at lower temperatures, the pinning effect is enhanced and a smaller grain size is obtained. According to our results, changing the volume fraction of inclusions results in achieving the optimal size of austenite grains. Moreover, the increasing of temperature would provide more energy for the grain to conquer the pinning forces of the inclusion. In summary, the results of this work show that the austenitization temperature, austenitization time, and inclusion volume fraction can be considered as three important parameters influencing the austenite grain size.

Acknowledgments: The work was financially supported by National Cheng Kung University in Taiwan. Special thanks to Dr. Y.H. Su, Iron and Steel Research and Development Department of China Steel Corporation, who gave us a lot of suggestions to promote our research. He supported us in all stages in experimental part.

Author Contributions: The experimental section was conducted by Zary Adabavazeh, PhD candidate in National Cheng Kung University; Amir Reza Ansari Dezfoli and Zary Adabavazeh collaborated on the simulation procedure; and Prof. Weng-Sing Hwang was the advisor.

Conflicts of Interest: The authors declare no conflict of interest.

References

1. Chang, P.-H.; Teng, T.-L. Numerical and experimental investigations on the residual stresses of the butt-welded joints. *Comp. Mater. Sci.* **2004**, *29*, 511–522. [[CrossRef](#)]
2. Dossett, J.; Totten, G.E. Steel heat treating fundamentals and processes, press quenching. In *ASM Handbook*; ASM International: Kinsman, OH, USA, 2013; Volume 4a, pp. 252–256.
3. Nichols, R. Quenching and tempering of welded carbon steel tubulars. *Fabricator (USA)* **1998**, *28*, 54–59.
4. Jacot, A.; Rappaz, M. A combined model for the description of austenitization, homogenization and grain growth in hypoeutectoid Fe-C steels during heating. *Acta Mater.* **1999**, *47*, 1645–1651. [[CrossRef](#)]
5. Danon, A.; Servant, C.; Alamo, A.; Brachet, J. Heterogeneous austenite grain growth in 9Cr martensitic steels: Influence of the heating rate and the austenitization temperature. *Mater. Sci. Eng. A* **2003**, *348*, 122–132. [[CrossRef](#)]
6. SEKI, A.; Sawada, M.; Moriguchi, K.; Shirai, Y. *Simulations of Grain Growth in Titanium and Stainless Steels; No. 106*; Nippon Steel & Sumitomo Metal Technical Report: Tokyo, Japan, July 2014.
7. Lee, S.-J.; Lee, Y.-K. Prediction of austenite grain growth during austenitization of low alloy steels. *Mater. Des.* **2008**, *29*, 1840–1844. [[CrossRef](#)]
8. Raghavan, S.; Sahay, S.S. Modeling the grain growth kinetics by cellular automaton. *Mater. Sci. Eng. A* **2007**, *445*, 203–209. [[CrossRef](#)]
9. Umamoto, M.; Ohtsuka, H.; Tamura, I. Grain size estimation from transformation kinetics. *Acta Metall.* **1986**, *34*, 1377–1385. [[CrossRef](#)]
10. Lai, G.; Wood, W.; Clark, R.; Zackay, V.; Parker, E. The effect of austenitizing temperature on the microstructure and mechanical properties of as-quenched 4340 steel. *Metall. Trans.* **1974**, *5*, 1663–1670. [[CrossRef](#)]
11. Kop, T.A.; Remijn, P.; Sietsma, J.; van der Zwaag, S. The effect of the austenitisation temperature on the transformation kinetics of an Nb-containing steel. *Mater. Sci. Forum* **1998**, *284–286*, 193–200. [[CrossRef](#)]
12. Vanherpe, L.; Moelans, N.; Blanpain, B.; Vandewalle, S. Pinning effect of spheroid second-phase particles on grain growth studied by three-dimensional phase-field simulations. *Comp. Mater. Sci.* **2010**, *49*, 340–350. [[CrossRef](#)]
13. Fan, D.; Chen, L.-Q. Computer simulation of grain growth using a continuum field model. *Acta Mater.* **1997**, *45*, 611–622. [[CrossRef](#)]
14. Moelans, N.; Blanpain, B.; Wollants, P. Pinning effect of second-phase particles on grain growth in polycrystalline films studied by 3-d phase field simulations. *Acta Mater.* **2007**, *55*, 2173–2182. [[CrossRef](#)]
15. Wang, L.; Qian, D.; Guo, J.; Pan, Y. Austenite grain growth behavior of AISI 4140 alloy steel. *Adv. Mech. Eng.* **2013**, *5*, 762890. [[CrossRef](#)]
16. Adabavazeh, Z.; Hwang, W.; Su, Y. Effect of adding cerium on microstructure and morphology of Ce-based inclusions formed in low-carbon steel. *Sci. Rep.* **2017**, *7*, 46503. [[CrossRef](#)] [[PubMed](#)]
17. Schmid, A. A time dependent Ginzburg-Landau equation and its application to the problem of resistivity in the mixed state. *Phys. Kondens. Mater.* **1966**, *5*, 302–317. [[CrossRef](#)]
18. Humphreys, F.J.; Hatherly, M. *Recrystallization and Related Annealing Phenomena*; Elsevier: Amsterdam, The Netherlands, 2012.
19. Liu, Y.; Patterson, B.R. Particle volume fraction dependence in zener drag. *Scr. Metall. Mater.* **1993**, *29*, 1101–1106. [[CrossRef](#)]
20. Smith, C. Zener pinning. *Trans. Met. Soc. AIME* **1948**, *175*, 15–51.
21. PA, M.; Ferry, M.; Chandra, T. Five decades of the zener equation. *ISIJ Int.* **1998**, *38*, 913–924.
22. Maalekian, M.; Radis, R.; Militzer, M.; Moreau, A.; Poole, W. In situ measurement and modelling of austenite grain growth in a Ti/Nb microalloyed steel. *Acta Mater.* **2012**, *60*, 1015–1026. [[CrossRef](#)]

